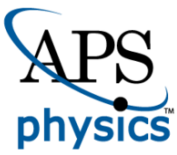

Quantum Interferences in Ultraclean Carbon Nanotubes

Neda Lotfizadeh, Mitchell J. Senger, Daniel R. McCulley, Ethan D. Minot, and Vikram V. Deshpande

Phys. Rev. Lett. **126**, 216802 — Published 26 May 2021

DOI: 10.1103/PhysRevLett.126.216802

Quantum Interferences in Ultraclean Carbon Nanotubes

Neda Lotfizadeh[1], Mitchell J. Senger[2], Daniel R. McCulley[2], Ethan D. Minot[2*] and Vikram V. Deshpande[1*]

[1]Department of Physics and Astronomy, University of Utah, Salt Lake City, Utah 84112, USA.

[2]Department of Physics, Oregon State University, Corvallis, OR 97331, USA.

*Correspondence to: vdesh@physics.utah.edu, ethan.minot@oregonstate.edu

Electronic analogues of optical interferences are a powerful tool to investigate quantum phenomena in condensed matter. In carbon nanotubes (CNTs), it is well established that an electronic Fabry-Perot interferometer can be realized. Other types of quantum interferences should also arise in CNTs, but have proven challenging to realize. In particular, CNTs have been identified as a system to realize the electronic analogue of a Sagnac interferometer - the most sensitive optical interferometer. To realize this Sagnac effect, interference between non-identical transmission channels in a single CNT must be observed. Here, we use suspended, ultra-clean CNTs of known chiral index to study both Fabry-Perot and Sagnac electron interferences. We verify theoretical predictions for the behavior of Sagnac oscillations and the persistence of the Sagnac oscillations at high temperatures. As suggested by existing theoretical studies, our results show that these quantum interferences may be used for electronic structure characterization of carbon nanotubes and the study of many-body effects in these model one-dimensional systems.

Quantum interferences of electron waves in devices with size close to the electron's coherence length have been instrumental in revealing various quantum and interaction effects [1–6]. Electronic analogues of Fabry-Perot [7] and Mach-Zehnder [8] interferometers have

stimulated extensive research over the past two decades [9–13]. Fabry-Perot (FP) interference was experimentally discovered in single-wall CNTs as conductance oscillations as a function of a nearby gate voltage [7] and has been the subject of numerous subsequent studies. In addition to the FP interference, previous theoretical studies have predicted the possibility of other quantum interference effects in CNTs with open contacts [12,14–17]. Refael et al. and Bishara et al. [14,15] proposed the electronic analogue of the Sagnac interferometer in CNTs, resulting from the interference between electron paths in two different subbands (K and K′) with different phase velocity. A recent quantum interference experiment by Dirnaichner et al. revealed this asymmetry between the K and K′ subbands [12]. The authors measured conductance versus gate voltage characteristics of a long suspended CNT. After averaging over FP oscillations, they found a long-period oscillation pattern that is consistent K and K′ subband asymmetry. Dirnaichner et al. proposed that this oscillation can be used to extract information about the chiral angle of the CNT. However, due to the lack of structural information of their nanotube, the accuracy of the proposed theory was not determined.

While the study by Dirnaichner et al. [12] gives preliminary evidence for K-K′ interference in a CNT, several questions remain to explore. First, alternative explanations for long-period conductance oscillations should be excluded. For example, a pair of weakly scattering defects in the CNT channel could produce long-period conductance oscillations. Second, competing models for the quantum interference should be tested. The Sagnac model [15] postulates that electron waves are split at the contacts between K and K′ paths, analogous to an optical beam splitter. In contrast, the secondary interference model [12] requires back reflections at the contacts such that FP-type interference can evolve independently on different interferometer paths. These different models predict different periods for the conductance oscillations (differing by a factor 2). Third,

the chirality dependence of long-period conductance oscillations has not been investigated. Lastly, the temperature dependence of the quantum interference contrast can reveal important physics. For example, electron-electron interactions are predicted to modify the temperature dependence of conductance oscillations caused by Sagnac interference [15].

Here, we verify the signature of electronic Sagnac interference in CNTs by measuring length-, structure-, and temperature-dependent interference patterns in long, ultraclean suspended CNTs. We use CNTs of known chiral index to show that the Sagnac oscillation period can be used to estimate the CNT chiral angle, consistent with the available theories [12,16]. We tune the length of the 1d channel to show that the period of a Sagnac oscillation increases as channel length decreases. We show that Sagnac oscillations persist at temperatures as high as 60K, whereas FP oscillations subside beyond ~10K. Finally, from the temperature dependence of Sagnac oscillations, we obtain information regarding interactions in CNTs.

Early studies of interference phenomena in CNTs focused on devices with channel lengths of a few hundred nanometers [7,18,19]. Although the FP interference can be observed in such devices, the Sagnac interference is missing from these reports since the predicted period of Sagnac oscillations is outside the accessible range of V_g. By studying a long CNT ($L \cong 1\mu m$) with highly transparent contacts, Dirnaichner et al. [12] pioneered the effort to study mesoscopic transport phenomena in long, ultraclean, open systems with transparent contacts. This new regime has not been comprehensively explored and our current study addresses this deficit in the CNT literature. Furthermore, our longer nanotubes ($L > 2$ μm) allow for optical characterization of CNT structure and, therefore, investigations of chirality-dependent properties.

To observe electron interference effects in CNTs we have constructed gate-tunable CNT channels that are free of disorder and have highly transparent contacts. To eliminate disorder, we

grow suspended CNTs as the final step of fabrication [20–26]. Details of our growth process are provided in previously published works [27,28]. Such devices have unveiled phenomena that were previously masked by disorder [22–24,26,27]. Fig. 1a shows a scanning electron microscopy image of a representative CNT. Our nanotubes are suspended over a ~2μm trench, with two gates located at the bottom of the trench (Fig. S1).

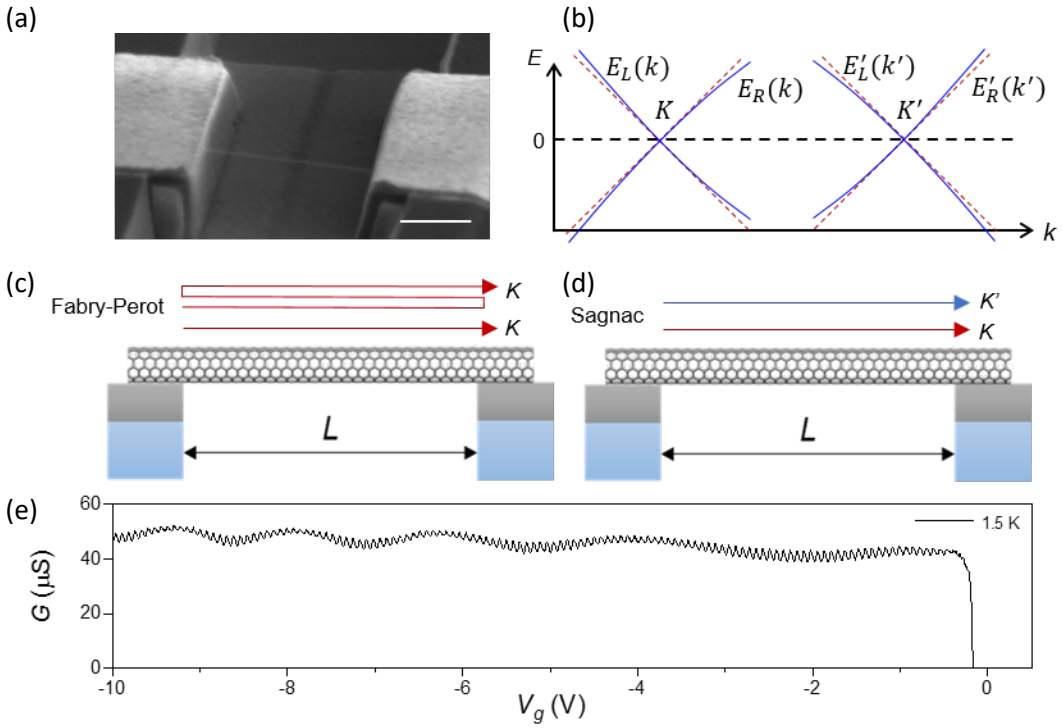

Fig. 1. (a) Scanning electron microscope image of a suspended CNT, scale bar is 1 μm. (b) Energy spectrum of left-moving (L) and right-moving (R) carriers in two sub-bands. Geometries for realizing Fabry-Perot (c) and (d) Sagnac interferences in CNT waveguide. Red (blue) arrows represent electron traveling in the K (K′) sub-band. (e) Conductance (G) versus V_g at T = 1.5K for D1 with ~2μm length.

Fabry-Perot interference can be produced by weak reflections of electron waves at the interface between the CNT and the metal contacts [7]. A direct propagating wave interferes with a scattered electron wave as shown in Fig. 1c. The phase difference between the two paths (Fig.

1c) is $\Delta\varphi_{\mathrm{FP}} = 2kL$ where k is the electron momentum in the K sub-band, and L is the length of the nanotube channel [7]. Fabry-Perot interference can also involve the K′ sub-band (not shown). Sagnac interference is illustrated in Fig. 1d. In this case, the interference occurs between direct paths in the K and K′ sub-bands. Asymmetry between the two sub-bands leads to the non-zero phase difference $\Delta\varphi_{\mathrm{S}} = (k - k')L$, where k' is the electron momentum in the K′ sub-band [14,15]. Both FP and Sagnac interferences, can be observed in experiment by measuring oscillations in device conductance as a function of Fermi energy.

To predict the period of conductance oscillations, consider the band structure of a metallic CNT. Fig. 1b shows the dispersion relationships for left-moving (L) and right-moving (R) carriers in the K and K′ sub-bands. The dashed lines show the linear dispersion approximation which is most commonly used in the CNT literature. The solid lines illustrate the small (but nevertheless observable) deviation from linear dispersion. For example, right-movers in the K sub-band are described by:

$$E_R(k) = \hbar v_{\mathrm{F}} k - \beta k^2 + \mathcal{O}(k^3) \qquad (1)$$

where E_{R} and k are measured relative to the Dirac point, v_{F} is a constant describing the carrier velocity at the Dirac point (tight-binding calculations predict $\hbar v_{\mathrm{F}} \approx 0.65\mathrm{eV.nm}$ [7]), and β is a constant that depends on the chiral angle of the CNT, θ [29]. Our tight-binding calculations predict that $\beta = [0.023\ \mathrm{eV} \cdot \mathrm{nm}^2] \cdot \sin 3\theta$ (see Supplemental Material [30]). Higher order terms, $\mathcal{O}(k^3)$, are too small to be relevant for our experiments. The set of four dispersion curves (Fig. 1b) satisfy electron-hole symmetry and time-reversal symmetry.

Using the band structure shown in Fig. 1b, one can calculate the phase differences $\Delta\varphi_{\mathrm{FP}}$ and $\Delta\varphi_{\mathrm{S}}$ for charge carriers at the Fermi energy, E_{F}. The phase difference $\Delta\varphi_{\mathrm{FP}}(E_{\mathrm{F}})$ and $\Delta\varphi_{\mathrm{S}}(E_{\mathrm{F}})$ will cause oscillations in zero-bias conductance described by:

$$G(E_{\mathrm{F}}) = G_{\mathrm{avg}} + A_{\mathrm{FP}} \cos\left(\frac{2LE_{\mathrm{F}}}{\hbar v_{\mathrm{F}}}\right), \qquad (2)$$

$$G(E_F) = G_{\mathrm{avg}} + A_{\mathrm{S}} \cos\left(\frac{2\beta L E_{\mathrm{F}}^2}{(\hbar v_{\mathrm{F}})^3}\right), \qquad (3)$$

where A_{FP} and A_{S} are amplitudes of the FP and Sagnac oscillations respectively. In Eq. 3, the factor E_{F}^2 causes the oscillation period to change with energy (as noted previously by Jiang et al. [16]). Given the expected values of L, β and v_{F}, we expect the period of Sagnac oscillations (Eq. 3) to be significantly longer than the period of FP for experimentally accessible values of E_{F}. The amplitude A_{FP} is determined by reflection coefficients at the contacts (for details see Ref [12]), whereas A_{S} depends on the coherent splitting of the electron beam at the contacts into the K and K′ valleys. If both FP and Sagnac interferences occur at the same time, we expect a superposition of these two oscillation patterns.

Figure 1e shows the conductance of a device D1 as a function of V_{g} at T=1.5K. The regularity and stability of our data indicates that our devices are high-quality and defect-free. The observed fast oscillations in conductance of D1 (period ~80mV) have a constant period over a wide range of V_{g}, consistent with the prediction of FP interference (Eq. 2). The observed slow oscillations have a much longer period that changes with V_{g}, consistent with the prediction of Sagnac interference (Eq. 3). We have observed this combination of constant-period fast oscillations, and variable-period slow oscillations in over 40 nanotube devices. We have

undertaken several experiments, described below, to verify that a combination of FP and Sagnac interference is generating these conductance oscillations.

We first verified that the conductance oscillations can be tuned by changing the channel length. First, E_F was varied in the full length of the CNT by operating both gate electrodes as a single gate (Fig. 2a, black curve). Next, E_F was tuned in half the CNT by holding one gate at a large fixed voltage and varying the voltage of the other gate (red curve). In this half-length configuration, a high-transparency tunnel barrier was created in the center of CNT [31]. Figure 2b&c show differential conductance, dI/dV_{sd}, plots for the full length and half length respectively. The differential conductance forms a rhombic pattern with a height of V_c=1.3mV (full-length) or V_c=2.1mV (half-length). Similar rhombic patterns have been observed previously and attributed to FP interference [7].

Figure 2 illustrates that both interference patterns (slow and fast oscillations) are tuned by channel length. Assuming the fast oscillation is caused by FP, Eq. 2 predicts that the oscillation period will scale inversely with L. Indeed, we find that the fast oscillation has a period of 80mV (full length), which increases to 170mV (half length). Similarly, if the slow oscillation is caused by Sagnac interference, the increased period of slow oscillation is expected to be consistent with Eq. 3. The cycle of the slow oscillation marked with arrows in Fig. 2a., has a period of ~2.47V (full length), which increases to ~4.1V (half length). In the Supplemental Material [30] we provide further quantitative analysis, accounting for the role of the gate lever arm, $\alpha = V_c/\Delta V_g^{FP}$ [7], to verify quantitative agreement with the predicted length dependence (Eq. 2 and 3). The key conclusion from Fig. 2 is that the observed interference effects can be attributed to scattering/mixing at the channel ends, and not to fixed scattering sites along the length of the channel.

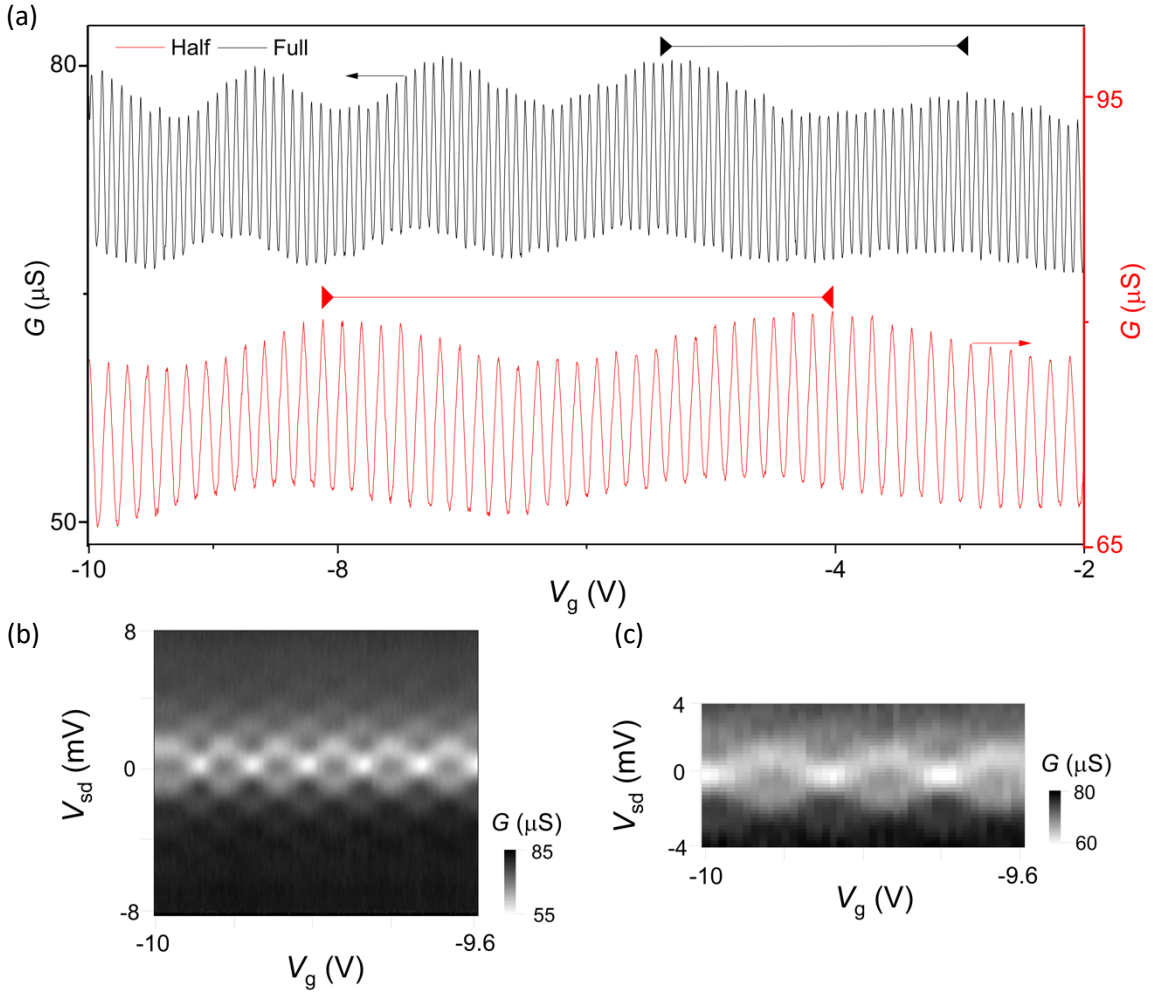

Fig. 2. (a) Conductance (G) versus V_g at T = 1.5K for whole (black) and half-length (red) of D2. Grayscale plot of differential conductance versus V_g and source-drain bias V_{sd} for (b) whole and (c) half-length of D2.

After establishing the length dependence of the interference patterns, we performed experiments on six CNTs of known chiral index (D3-D8). Chiral index was determined using scanning photocurrent spectroscopy to characterize the devices (see Supplemental Material [30]). A representative photocurrent spectrum is shown in Fig. 3a (see also Fig. S4). The chiral angles of the six CNTs ranged from θ = 16.1° to 30°. We also used photocurrent microscopy to determine the length of the suspended CNT [30]. Fig. 3b shows the conductance oscillations measured in these six CNTs. The red dashed lines show the fit functions that are based on Eq. 3:

$$G = G_{\text{avg}} + A_{\text{S}} \cos\left(\gamma \left(V_{\text{g}} - V_{\text{g,0}}\right)^2\right) \qquad (4)$$

where G_{avg} describes the average conductance and A_s the amplitude of the oscillation. Here G_{avg}, A_s, γ and V_{g0} are treated as fit parameters for each device. The periodicity of the measured oscillations is well described by the $\cos(V_g^2)$ dependence.

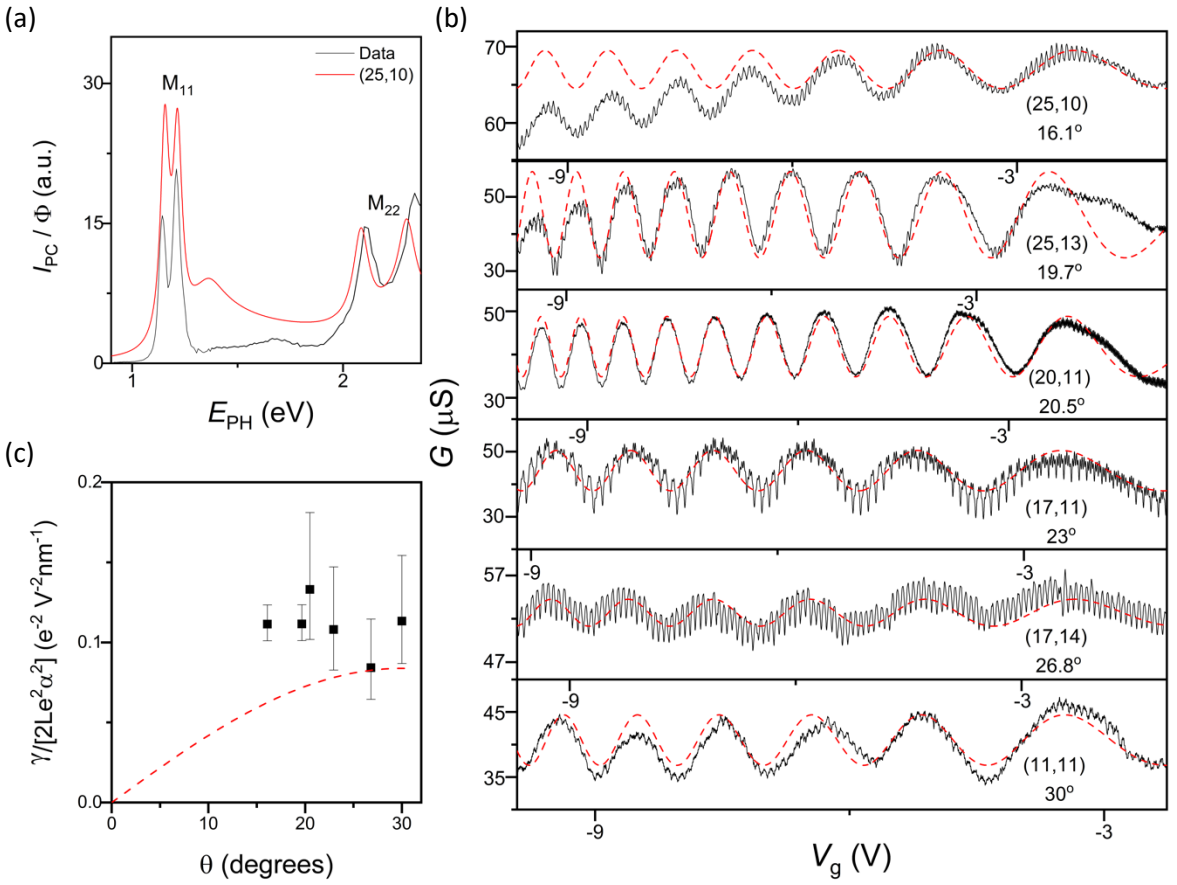

Fig. 3. (a) Photocurrent spectrum of D3 (25, 10) and fit to excitonic model. (b) Experimental data (black) and fit functions (red) of conductance versus V_g. The measured chiral index is noted for each device. (c) Comparison of measured (dots) and calculated (red line) of $\gamma/(2Le^2\alpha^2)$ as a function of θ for the six CNTs.

The relative amplitude of fast and slow oscillations varies between devices. This is consistent with the FP and Sagnac mechanisms; A_{FP} is determined by reflection coefficients at the

contacts, whereas A_s is determined by channel splitting at the contacts. If the slow oscillations are caused by Sagnac interference, Eq. 3 predicts that the fitting parameter γ will be given by:

$$\gamma = \frac{2Le^2\alpha^2\beta}{(\hbar v_F)^3} \approx \frac{2Le^2\alpha^2 \cdot [0.023\ \text{eV} \cdot \text{nm}^2] \cdot \sin(3\theta)}{[0.65\ \text{eV} \cdot \text{nm}]^3} \qquad (5)$$

The second equality uses the values of β and $\hbar v_F$ from tight-binding calculations. To compare our measurements with theory, we plot $\gamma/(2Le^2\alpha^2)$ as a function of θ for the six CNTs (Fig. 3c). We assume that L is equal to the suspended length of the CNT determined from photocurrent microscopy. In two devices, α was determined from differential conductance measurements (the mean value was 0.028 and the difference was 0.004). The exact value of α is unknown in four devices, therefore, we assumed $\alpha = 0.028 \pm 0.004$ for them.

Figure 3c shows that the measured γ parameter (normalized for length and gate lever arm) is approximately 30% larger than predicted by tight-binding parameters (Eq. 5). It is possible that strong electron-electron interactions in the CNT modify the band structure so that tight-binding calculations are a poor description of our system. Despite this 30% discrepancy, the approximate agreement between measured and predicted $\gamma/(2Le^2\alpha^2)$, is sufficient to increase our confidence in the proposed Sagnac interference mechanism.

The measurements shown in Fig. 3c are not precise enough to verify the expected sin(3θ) dependence. Further experiments with a wider range of θ, and with precise characterization of L and α, are required. We speculate that future work will refine this characterization method to reach a precision that enables researchers to determine θ from quantum interference patterns. There is one caveat, however, the sin(3θ) function is flat when θ = 30°. Therefore, the method will not be suitable for distinguishing chiral angles that are close to 30°.

As a final test of the electron interference mechanisms, we measured the temperature dependence of the interference contrast. Fig. 4a shows the evolution of conductance oscillations as the temperature is increased from 2.25K to 30K. The fast oscillations disappear at ~7K while slow oscillations survive up to 30K. Slow oscillations survived as high as 60K in other devices (see Fig. S5 [30]).

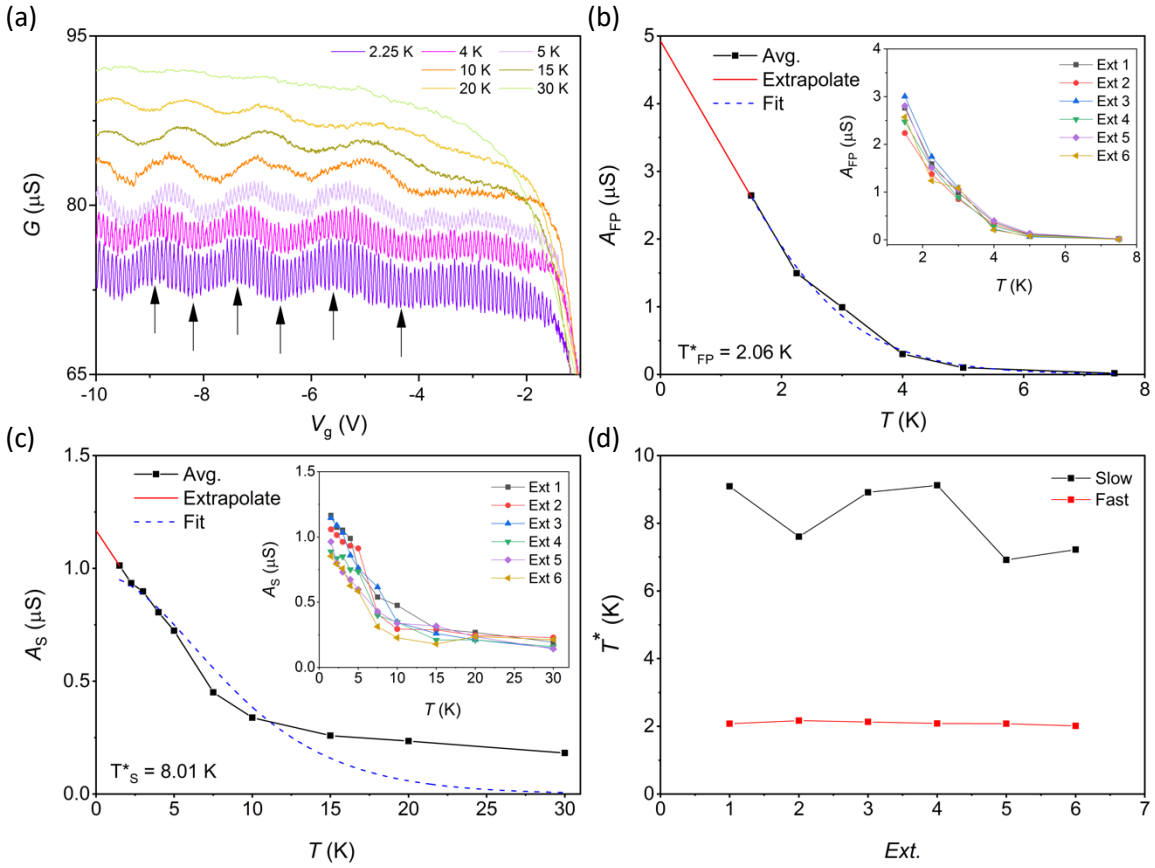

Fig. 4. (a) Temperature dependence of the conductance of D2 as a function of V_g. Black arrows show the extremum points (Ext) of the slow oscillation. Averaged amplitudes of (b) fast and (c) slow oscillations over the whole range of V_g calculated using FFT over a sliding window of 0.75V as a function of temperature. Dashed blue line is a fit to Eq. (6) in the text, and red line is an extrapolate to $T = 0\ K$. Insets: Amplitude of (b) fast and (c) slow oscillations at Ext of slow oscillation vs. temperature. (d) T^* of fast (red) and slow (black) oscillations at Ext of slow oscillation, here T^* is a temperature at which $A\ (T^*) =\ \exp\ (-1) \cdot A\ (T = 0)$.

The temperature dependence in Fig. 4a is consistent with fast oscillations caused by the FP mechanism and slow oscillations by the Sagnac mechanism. At finite temperature, interference contrast will be reduced by the thermal spread of electron energies. Contrast is lost completely when the thermal energy, $\sim k_B T$, causes a 2π spread in the phase difference $\Delta\varphi_{\mathrm{FP}}$ or $\Delta\varphi_{\mathrm{S}}$. For FP interference, $\Delta\varphi_{\mathrm{FP}}$ changes rapidly with electron energy, which results in a low temperature threshold for losing interference contrast. For a channel length L=2μm, the expected temperature threshold for FP oscillations is a few Kelvin ($T_{\mathrm{FP}} \approx \pi\hbar v_{\mathrm{F}}/(Lk_B)$). For Sagnac interference, $\Delta\varphi_{\mathrm{S}}$ changes more slowly with electron energy and the expected temperature threshold is significantly higher.

To analyze the temperature dependence in more detail, the oscillation amplitudes were calculated by performing a fast Fourier transform (FFT) over a sliding window of 0.75V at each temperature. Amplitudes of fast and slow oscillations averaged over the whole range of V_{g} are plotted as a function of temperature in Fig. 4b and c. The amplitude of FP interference A_{FP}, is expected to follow a temperature behavior of [15,32]:

$$A_{FP}(T) \sim A_{FP}(T=0) \cdot \left(\frac{T}{\sinh\left(\frac{2\pi k_B L T}{\hbar v_F}\right)} \right) \tag{6}$$

It can be seen from Fig. 4b that amplitudes of our fast oscillations fit very well (dashed blue line) to Eq. 6. Bishara et al. [15] predicted that the amplitude of Sagnac oscillation in non-interacting nanotubes follow a similar relationship to Eq. 6. They modified Eq. 6 by multiplying T by a factor $\frac{u}{v_{\mathrm{F}}}$, where $u = \hbar^{-1}(dE/dk - dE'/dk') \approx \frac{4\beta E}{\hbar^2 v_{\mathrm{F}}}$ is the velocity difference between electrons with energy E in the K and K′ sub-bands. Since $u \ll v_F$, the non-interacting theory predicts that Sagnac oscillations persist to much higher temperatures than FP oscillations [15]. Indeed, we observe this

higher temperature threshold for Sagnac oscillations. However, the functional form of the temperature dependence does not follow the inverse *sinh* relationship that is predicted by the non-interacting theory (Fig. 4c, dashed blue line). Moreover, the temperature dependence does not change significantly as u is modified by tuning the Fermi energy (Fig. 4c inset).

To explain the deviation from the inverse *sinh* relationship, we consider the role of Coulomb interactions [15]. The inset of Fig. 4c shows the Sagnac oscillation amplitude at each extremum of the Sagnac oscillation (the extrema are indicated by black arrows in Fig. 4a, with extremum 1 located closest to charge neutrality). The Sagnac oscillation amplitude is almost independent of V_g and, therefore, almost independent of u. Bishara predicted that Sagnac oscillations will show such behavior in the strongly interacting regime, i.e. Luttinger liquid parameter $g \leq 0.5$ [15]. The equivalent of Eq. (6) for interacting nanotubes was non-trivial to obtain, therefore, Bishara considered the temperature T^* at which the amplitude of oscillations became a factor $1/e$ of their zero-temperature amplitude. In the strongly interacting regime, Bishara predicted that Sagnac oscillations are characterized by T_S^* which is weakly dependent on u and g, and that $T_S^* \approx 7T_{FP}^*$. Figure 4d shows the experimentally determined values of T_S^* and T_{FP}^* obtained at the extremum points. We find $T_S^*/T_{FP}^*, \approx 4-5$, slightly less than predicted by Bishara. In other devices (Fig. S6), we found $T_S^*/T_{FP}^* \approx 4-7$. It is possible that this variation in T_S^*/T_{FP}^* is due to a non-negligible dependence on u and g, even in the strongly interacting regime. This possibility warrants further theoretical investigation. We conclude that Sagnac interference provides information on electron interactions in CNTs, and the temperature dependence of Sagnac interference may reveal the interaction strength parameter.

In summary, we studied two forms of quantum interference in long, suspended ultra-clean CNTs. Fabry-Perot interference is manifested as rapid oscillations in CNT conductance. A slower,

conductance oscillation is identified as arising from Sagnac interference. While the FP mechanism involves an electron path that traverses the CNT channel multiple times, the Sagnac mechanism involves paths that traverse the channel only once, but in different sub-bands. Using theoretical modeling and experiments on devices with known chiral indices, we verified that the Sagnac oscillation patterns are consistent with theory. Future measurements of CNTs may use such quantum interference measurements to determine CNT chiral angle – circumventing the need for optical characterization or atomic-resolution imaging. Lastly, by studying the temperature dependence of the interference effects in nanotubes, we showed that Sagnac interference can provide information on the interaction effects in these devices.

Acknowledgments

Work performed in Utah was supported in part by the National Science Foundation under Grant No. 2005182. Work performed in Oregon was supported by the National Science Foundation under Grant No. 1709800. A portion of device fabrication was carried out in the University of California Santa Barbara (UCSB) nanofabrication facility. Part of this research was conducted at the Northwest Nanotechnology Infrastructure, a National Nanotechnology Coordinated Infrastructure site at Oregon State University which is supported in part by the National Science Foundation (grant ECCS-1542101) and Oregon State University. The authors would like to thank Wataru Izumida and Massimo Rontani for helpful discussions.

Competing interests

The authors declare no competing interests.

[1] S. Chen, Z. Han, M. M. Elahi, K. M. M. Habib, L. Wang, B. Wen, Y. Gao, T. Taniguchi, K. Watanabe, J. Hone, A. W. Ghosh, and C. R. Dean, Science **353**, 1522 (2016).

[2] D. S. Wei, T. van der Sar, J. D. Sanchez-Yamagishi, K. Watanabe, T. Taniguchi, P. Jarillo-Herrero, B. I. Halperin, and A. Yacoby, Science Advances **3**, e1700600 (2017).

[3] A. W. Barnard, A. Hughes, A. L. Sharpe, K. Watanabe, T. Taniguchi, and D. Goldhaber-Gordon, Nature Communications **8**, 15418 (2017).

[4] C. Handschin, P. Makk, P. Rickhaus, M. H. Liu, K. Watanabe, T. Taniguchi, K. Richter, and C. Schönenberger, Nano Letters **17**, 328 (2017).

[5] J. Li, R. X. Zhang, Z. Yin, J. Zhang, K. Watanabe, T. Taniguchi, C. Liu, and J. Zhu, Science **362**, 1149 (2018).

[6] D. T. McClure, W. Chang, C. M. Marcus, L. N. Pfeiffer, and K. W. West, Physical Review Letters **108**, 256804 (2012).

[7] W. Liang, M. Bockrath, D. Bozovic, J. H. Hafner, M. Tinkham, and H. Park, Nature **411**, 665 (2001).

[8] Y. Ji, Y. Chung, D. Sprinzak, M. Heiblum, D. Mahalu, and H. Shtrikman, Nature **422**, 415 (2003).

[9] I. Neder, M. Heiblum, Y. Levinson, D. Mahalu, and V. Umansky, Physical Review Letters **96**, 016804 (2006).

[10] L. V. Litvin, H. P. Tranitz, W. Wegscheider, and C. Strunk, Physical Review B **75**, 033315 (2007).

[11] N. Y. Kim, P. Recher, W. D. Oliver, Y. Yamamoto, J. Kong, and H. Dai, Physical Review Letters **99**, 036802 (2007).

[12] A. Dirnaichner, M. del Valle, K. J. G. Götz, F. J. Schupp, N. Paradiso, M. Grifoni, C. Strunk, and A. K. Hüttel, Physical Review Letters **117**, 166804 (2016).

[13] W. Yang, C. Urgell, S. L. D. Bonis, M. Marganska, M. Grifoni, and A. Bachtold, Physical Review Letters **125**, 187701 (2020).

[14] G. Refael, J. Heo, and M. Bockrath, Physical Review Letters **98**, 246803 (2007).

[15] W. Bishara, G. Refael, and M. Bockrath, Physical Review B **78**, 165405 (2008).

[16] J. Jiang, J. Dong, and D. Y. Xing, Physical Review Letters **91**, 056802 (2003).

[17] L. Yang, J. Chen, H. Yang, and J. Dong, Physica Status Solidi (B) **242**, 1476 (2005).

[18] J. Kong, E. Yenilmez, T. W. Tombler, W. Kim, H. Dai, and R. B. Laughlin, Physical Review Letters **87**, 106801 (2001).

[19] J. Cao, Q. Wang, M. Rolandi, and H. Dai, Physical Review Letters **93**, 216803 (2004).

[20] B. J. LeRoy, S. G. Lemay, J. Kong, and C. Dekker, Applied Physics Letters **84**, 4280 (2004).

[21] J. Cao, Q. Wang, and H. Dai, Nature Materials **4**, 745 (2005).

[22] V. V. Deshpande and M. Bockrath, Nature Physics **4**, 314 (2008).

[23] F. Kuemmeth, S. Ilani, D. C. Ralph, and P. L. McEuen, Nature **452**, 448 (2008).

[24] G. A. Steele, A. K. Huttel, B. Witkamp, M. Poot, H. B. Meerwaldt, L. P. Kouwenhoven, and H. S. J. van der Zant, Science **325**, 1103 (2009).

[25] E. A. Laird, F. Kuemmeth, G. A. Steele, K. Grove-Rasmussen, J. Nygård, K. Flensberg, and L. P. Kouwenhoven, Reviews of Modern Physics **87**, 703 (2015).

[26] I. Shapir, A. Hamo, S. Pecker, C. P. Moca, Ö. Legeza, G. Zarand, and S. Ilani, Science **364**, 870 (2019).

[27] N. Lotfizadeh, D. R. McCulley, M. J. Senger, H. Fu, E. D. Minot, B. Skinner, and V. V. Deshpande, Phys. Rev. Lett. **123**, 197701 (2019).

[28] T. Sharf, J. W. Kevek, and E. D. Minot, 2011 11th IEEE International Conference on Nanotechnology (2011), pp. 122–125.

[29] R. Saito, G. Dresselhaus, and M. S. Dresselhaus, Physical Review B **61**, 2981 (2000).

[30] See Supplemental Material at [Url], Which Includes Refs. [33-37].

[31] G. A. Steele, G. Gotz, and L. P. Kouwenhoven, Nature Nanotechnology **4**, 363 (2009).

[32] P. Recher, N. Y. Kim, and Y. Yamamoto, Physical Review B **74**, 235438 (2006).

[33] K. Liu *et al.*, An atlas of carbon nanotube optical transitions. Nature Nanotechnology **7**, 325–329 (2012).

[34] K. Liu *et al.*, Proceedings of the National Academy of Sciences **111**, 7564–7569 (2014).

[35] T. DeBorde, L. Aspitarte, T. Sharf, J. W. Kevek, E. D. Minot, The Journal of Physical Chemistry C **118**, 9946–9950 (2014).

[36] M. J. Senger, D. R. McCulley, N. Lotfizadeh, V. V. Deshpande, and E. D. Minot, Physical Review B **97**, 035445 (2018).

[37] L. Aspitarte, D. R. McCulley, E. D. Minot, Nano Letters **16**, 5589–5593 (2016).